Growth and properties of high index Ta_2O_5 optical coatings prepared by HiPIMS and other methods

M. Hála[a], R. Vernhes[a], O. Zabeida[a], E. Bousser[a], J.E. Klemberg-Sapieha[a], R. Sargent[b], and L. Martinu[a,*]

[a]*Department of Engineering Physics, Thin Film Research Center – GCM, Polytechnique Montreal, P.O. Box 6079, Station Centre-Ville, Montreal, Quebec H3C 3A7, Canada*
[b]*JDSU, Santa Rosa, CA, USA*

Abstract

In the present work, we investigate amorphous Ta_2O_5 films prepared using different magnetron sputtering techniques at a constant average power but under various power delivery conditions in the context of their application as high index material in optical coatings. We used a broad range of pulse frequencies and pulse durations, discharge voltage and current levels. This allowed us to systematically assess the effect of the specific deposition conditions on the growth characteristics, surface morphology, as well as on the optical and mechanical properties. In particular, we show that the HiPIMS-deposited films exhibit enhanced properties such as low surface roughness ($\sim 0.2\,\text{nm}$), low residual stress ($\sim -50\,\text{MPa}$), high refractive index ($n_{550} \sim 2.22$) and high hardness ($\sim 7.8\,\text{GPa}$). Some of these properties are found to be comparable with the values reported for fully dense thermally-grown films. The presented observations are discussed in terms of energetic conditions at the substrate level.

Keywords: Magnetron sputtering, Pulsed plasmas, Optical coatings, Thin films, Thin film characterization

---

* *Contact author:* Ludvik Martinu
Email address: Ludvik.Martinu@polymtl.ca
Tel.: 514-340-4099
Fax: 514-340-3218

1. Introduction

High power impulse magnetron sputtering (HiPIMS) is a physical vapor deposition (PVD) technique providing high ionization of the sputtered material available for the deposition process [1]. HiPIMS discharges were found to be beneficial in the deposition of single-layer, multilayer and nanocomposite protective coatings [2], and in substrate pre-treatment for adhesion enhancement [3]. More recently, HiPIMS has also been used in the preparation of various transparent metal oxides [4–14], of which many have shown improved characteristics.

For instance, in the context of optical coating applications, Nb_2O_5 [14] and Al_2O_3 [13] films grown by HiPIMS have exhibited higher refractive indices than those fabricated by other PVD techniques, as well as moderate internal stresses (lower than 150 MPa). More specifically, HiPIMS-deposited TiO_2 films were found to possess a higher film density and a higher refractive index in comparison to those obtained by direct current magnetron sputtering (DCMS) [5, 11] and pulsed-DCMS (PDCMS) [6], due to promoted growth of the rutile phase. Other reported advantages of films prepared by HiPIMS include a lower surface roughness [5, 7, 8] and, in the case of transparent conductive oxide (TCO) films, a lower resistivity [8, 9]. In addition, it has been documented that under certain conditions the HiPIMS process may be hysteresis-free [10, 13, 14], and can reach comparable or higher deposition rates than DCMS [4, 5, 13] or bipolar pulsed DCMS [7].

Despite the steadily increasing number of encouraging observations for HiPIMS deposited films, a systematic comparison of the overall coating performance with respect to the traditional deposition techniques such as DCMS and PDCMS is still missing. In the present work, we perform a rigorous investigation of the characteristics of Ta_2O_5 coatings prepared at a constant average power density (11 W/cm^2) but under various discharge conditions produced using HiPIMS, PDCMS and DCMS power supplies. We then discuss the evaluated deposition rates, surface morphologies, and optical and mechanical properties of this high refractive index metal oxide in the context of its use in optical interference coat-

ing systems. Finally, we propose an interpretation of the results based on the plasma characteristics and the energetic conditions at the substrate level.

2. Experimental details

2.1. Deposition system and fabrication conditions

All experiments were performed in a pilot vacuum deposition system consisting of a turbomolecularly pumped 700 l stainless steel chamber equipped with a circular 10 cm diameter magnetron (ONYX-4 HP, Angstrom Sciences Inc.) facing the substrate holder. The magnetron was loaded with a tantalum target (99.95 % purity) and was powered by either (i) a Solvix HiP^3 power supply that can be operated either in DC or HiPIMS mode, or (ii) a RÜBIG Micropulse MP 120 pulsed DC power supply. In the HiPIMS mode, the HiP^3 generator can operate in a frequency range from 5 Hz to 1 kHz at a voltage pulse duration between 10 μs and 400 μs, and with a maximum voltage and peak current of 1000 V and 600 A, respectively (5 kW maximum output power). The MP 120 power supply can deliver pulses 4 μs to 1000 μs long with a repetition frequency ranging from 1 kHz to 50 kHz and with a maximum voltage and peak current of 1000 V and 120 A.

The specific experimental conditions used in this work are listed in Table 1, together with the most important discharge characteristics of the respective depositions. In essence, we decreased the signal duty cycle from high to low values (DCMS: 100 %, PDCMS: 25 %, and HiPIMS: 5 % and 1 %) while increasing the pulse cathode voltage (U_C, from 510 to 860 V) in order to keep the average power density constant ($P_{da} = 11$ W cm^{-2}). This resulted in a ~100 times increase in the peak current density (J_C, from 0.02 to 1.70 A cm^{-2}) and a ~150 times increase in the peak power density (P_{dp}, from 0.01 to 1.46 kW cm^{-2}). The PDCMS discharge frequency was set to 10 kHz, which corresponds to a mid-frequency pulsed process. A lower frequency was used in HiPIMS (50 Hz and 1 kHz) in order to maintain the pulse length in the 100 μs range. Such a pulse length is necessary in order to fully develop the high plasma density discharge and to operate it in a hysteresis-free sputtering regime [14].

Table 1: Characteristics of the discharges used in the preparation of Ta_2O_5 coatings. All discharges were operated using a fixed average target power density (11 W/cm^2).

Type of discharge	DCMS	PDCMS 10 kHz	HiPIMS 1 kHz	HiPIMS 50 Hz	DCMS	HiPIMS 50 Hz
Power supply	Solvix HiP^3	Rübig MP120	Solvix HiP^3	Solvix HiP^3	Solvix HiP^3	Solvix HiP^3
Pulse frequency (kHz)	0	10	1	0.05	0	0.05
Pulse length (μs)	N/A	25	50	200	N/A	200
Duty cycle (%)	100	25	5	1	100	1
Cathode voltage (V)	510	640	750	860	560	970
Peak current density (A/cm^2)	0.02	0.10	0.47	1.70	0.02	2.24
Peak power density (kW/cm^2)	0.01	0.07	0.35	1.46	0.01	2.20
O_2/Ar flow ratio	0.4	0.4	0.4	0.4	1.7	1.7
Working pressure (Pa)	0.80	0.80	0.80	0.80	0.25	0.25

We carried out the experiments at two different working pressures, i.e. 0.25 Pa and 0.80 Pa, in order to evaluate the effect of this parameter on the deposition rate and on the Ta_2O_5 film properties. The gas flow ratios were kept constant at a given working pressure ($O_2/Ar = 0.4$ at 0.80 Pa and $O_2/Ar = 1.7$ at 0.25 Pa), and were specifically chosen to ensure good discharge stability while providing enough oxygen to produce transparent stoichiometric coatings by the two studied discharges. The base pressure in the chamber was less than 5×10^{-4} Pa prior to depositions.

The Ta_2O_5 films were deposited on both B270 glass and crystalline Si <100> substrates positioned at a distance of 15 cm from the target. No external heating or biasing was used and the substrate holder was maintained at floating potential. Deposition time was adjusted depending on the discharge conditions in order to keep the film thickness nearly constant at $1\,\mu m \pm 20\,\%$.

2.2. Discharge and film characterization

Waveforms of the target voltage, U_C, and of the instantaneous cathode current, I_C, were monitored by a Tektronix P6015A voltage probe and a Pearson 301X current probe, respectively, and recorded by a Tektronix DPO3014 digital oscilloscope. The average target power density, P_{da}, was then calculated as:

$$P_{da} = f/A_C \int_0^{T_C} U_C(t) I_C(t)\,dt, \qquad (1)$$

where f stands for the pulse repetition frequency, A_C for the cathode area ($A_C = 78\,cm^2$), t for time and T_C for the pulse duration during which the cathode current has a non-zero value. For experiments performed in the DCMS mode, the target voltage, current and power were directly obtained from the readout of the DC power supply.

In a similar fashion, the ion flux arriving at the substrate was evaluated by measuring the average current density at the substrate holder, J_{sa}, as:

$$J_{sa} = f/A_S \int_0^{T_S} I_S(t)\,dt, \qquad (2)$$

where I_S is the instantaneous current through the substrate holder shielded by a mask with an opening of known surface, $A_S = 4\,cm^2$, and T_S is the pulse duration during which the substrate current is positive. During the measurements of ion current density, the sample holder was biased to -100 V by a DC power supply (AE Pinnacle 6 kW) in order to suppress the flow of plasma electrons.

Optical characterization of the films was performed using a variable angle spectroscopic ellipsometer (RC2 instrument from J. A. Woollam Co.). Ellipsometric angles were measured at five angles of incidence (from 55° to 75° in 5° increments) with wavelengths ranging from 193 to 1690 nm. The ellipsometric data were then analyzed by the CompleteEASE software (J. A. Woollam Co.), allowing us to determine both the thickness, d, and the refractive index, n, of the studied films. The dispersion curves of the Ta_2O_5 material were modeled using the Tauc Lorentz equation [15]. Complementary absorbance measurements were performed with a Lambda19 double beam spectrophotometer (Perkin Elmer).

The film surface morphology was characterized by atomic force microscopy (AFM) using a Veeco Dimension 3100 instrument.

The hardness of the Ta_2O_5 films was evaluated by depth-sensing indentation (Hysitron Triboindenter) using a diamond tip of Berkovich geometry. The load function used for these indentations was trapezoidal with a 5 s loading segment followed by a 2 s holding segment, and finished with a 5 s unloading segment. The data were analyzed using the Oliver and Pharr methodology [16]. Prior to testing, the tip geometry and system compliance were calibrated using a fused silica standard and, before each indentation, the drift of the system was measured (typically less than 0.1 nm/s) and subtracted from the acquired data. In order to isolate the coating properties from the influence of the substrate, the hardness was evaluated as a function of depth in accordance with ISO standard 14577-4. Therefore, each coating was indented by five repetitions of a 5x5 indentation array with a spacing of 20 μm between indentations. The indentation load within each array was decreased incrementally from a maximum of 10 mN for the first indentation down to 0.1 mN for the last.

Finally, the internal stress of the coatings was evaluated by measuring the

curvature of rectangular Si strips ($10 \times 50\,\mathrm{mm}^2$) before and after film deposition in a stress measurement apparatus (Tencor FLX-2900). The value of the internal stress was calculated from the radius of curvature using the Stoney relation.

3. Results and discussion

The dependence of deposition rate (r) as a function of U_C is shown in Fig. 1a. At $p = 0.80\,\mathrm{Pa}$, all pulsed discharges exhibit a lower r compared to the DCMS discharge ($r_\mathrm{DCMS} = 8.2\,\mu\mathrm{m/h}$). The lowest r (about 25% of r_DCMS) is observed for the HiPIMS 50Hz discharge, which presents the highest instantaneous plasma density. There are several phenomena that can be responsible for this effect [19–22]: (i) loss of the sputtered material via ionization and subsequent back-attraction towards the target, (ii) less-than-linear dependence of the sputtering yield on the energy of bombarding ions, and (iii) modified target-substrate transport geometry. At $p = 0.25\,\mathrm{Pa}$, the deposition rate in the DCMS mode is twofold lower ($r_\mathrm{DCMS} = 4.0\,\mu\mathrm{m/h}$) but still higher than that in the HiPIMS mode ($r_\mathrm{HiPIMS} = 3.1\,\mu\mathrm{m/h}$). We believe that the drop of r in the DCMS mode is actually related to the higher O_2/Ar flow ratio employed at that pressure, which causes the target to enter the poisoned mode. On the contrary, these gas conditions seem to increase r in the HiPIMS mode, possibly due to a combination of self-cleaning effect at the target [14] and better material transport from target to substrate related to lower number of collisions in the gas phase [23]. It is also worth mentioning that the deposition rate can be significantly enhanced in the HiPIMS process by optimizing the magnetron's magnetic field strength at the target surface, as shown in our previous work [22]. In fact, it was previously documented that r of reactive HiPIMS can be comparable or even higher than that obtained with other frequently used PVD techniques operated at identical average current [5], or power [4, 7, 13].

In parallel to the deposition of Ta_2O_5 coatings, we have characterized the ion flux at the substrate holder for all pulsed discharges. Knowing the deposition rate, we could then determine the instantaneous ion to film-atom ratio, as plotted in Fig. 1b. (The DCMS values were estimated to be in the range of one

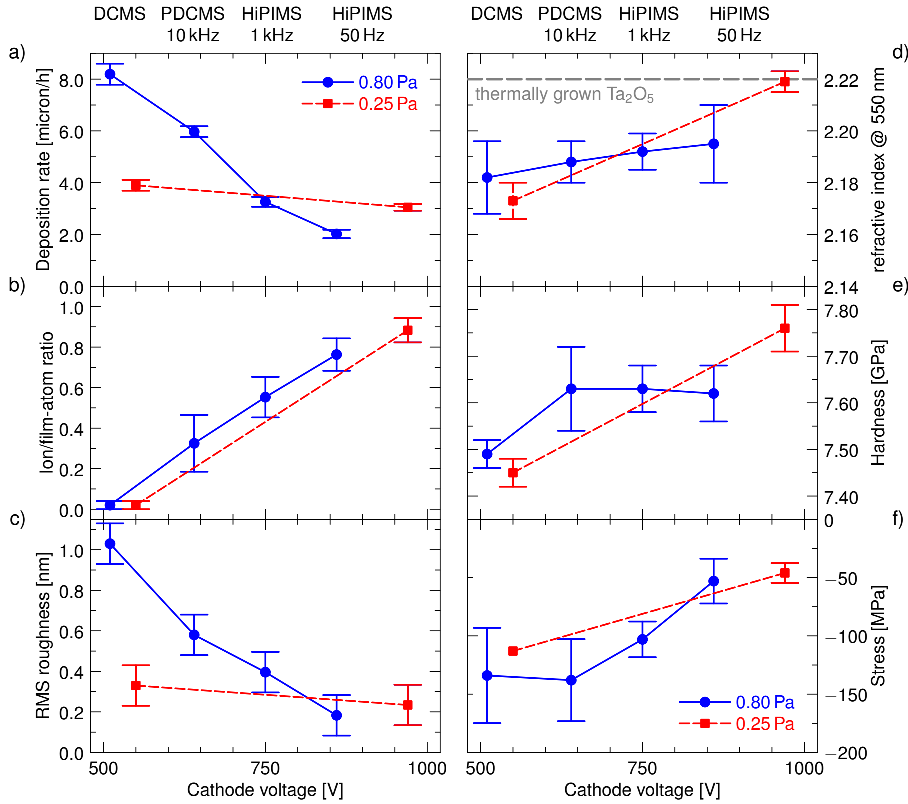

Figure 1: a) Deposition rate, b) ion to film-atom arrival ratio at the substrate level, c) surface roughness, d) index of refraction at 550 nm, e) hardness, and f) residual mechanical stress of Ta_2O_5 films as a function of the cathode voltage. The circle and square symbols stand for experiments at $p = 0.80$ Pa and $p = 0.25$ Pa, respectively. Each data point in figures a), d), e) and f) represents the average of measurements performed on three to four samples deposited using the same experimental conditions but during separate experiments, except for DCMS at $p = 0.25$ Pa representing two experiments only. The refractive index of thermally-grown amorphous Ta_2O_5 films is indicated for comparison [17, 18].

percent based on various references [24, 25].) The relatively high values of this ratio for HiPIMS discharges are not surprising, as suggested by previous experimental work on non-reactive HiPIMS process [22, 26, 27]. In fact, the average ionized fraction of sputtered metal in the flux onto the substrate can approach unity for certain materials, as indicated by modeling [19]. However, the exact role of the individual ionized working gas species (Ar^+, O^+ and O_2^+) has not been assessed at the moment. Higher energy per condensing atom brought by ions increases the film density which directly affects the film roughness, refractive index and hardness discussed below.

RMS roughness decreases substantially with U_C, as shown in Fig. 1c, where one can observe a direct correlation with the ion to film-atom ratio at the substrate (Fig. 1b). This is believed to be the case since as the actual discharge-driving voltage increases, condensing film atoms receive greater energy due to the localized heating provided by a higher portion of the incoming ions (including the ionized film atoms themselves). Consequently, these adatoms have higher surface mobility to find more energetically-favorable position on the underlying surface that maximize the number of bonds with their neighbors and thus minimize the resulting surface roughness.

Ta_2O_5 coatings prepared at $p = 0.80$ Pa present increasing refractive index values at 550 nm ($2.18 < n_{550} < 2.20$) versus U_C, as determined by ellipsometry (Fig. 1d). At $p = 0.25$ Pa, the refractive index of the HiPIMS deposited films is further increased up to 2.22. This value is significantly higher than those reported for Ta_2O_5 films prepared by both low- and high-energy PVD and plasma-based techniques, such as electron-beam evaporation ($n_{550} = 2.07$) [28], plasma enhanced chemical vapor deposition (PECVD) ($2.12 < n_{550} < 2.16$) [29], dual ion beam sputtering (DIBS) ($2.13 < n_{550} < 2.16$) [30], or pulsed laser deposition (PLD) ($n_{633} = 2.18$) [31]. In fact, only thermally-grown amorphous Ta_2O_5 films seem to possess comparable refractive index values: $n_{514} = 2.25$ [17] and $n_{633} = 2.20$ [18], as compared to $n_{514} = 2.24$ and $n_{633} = 2.20$ obtained in this work. This observation suggests that these films are exceptionally dense, because of a more intense ion bombardment related to increased U_C and due to

the reduced energy losses through collisions in the gas phase.

In order to verify that the observed elevated values of n cannot be ascribed to differences in the evaluation methodology, we measured by ellipsometry a reference Ta_2O_5 film fabricated by DIBS and we analyzed it using the same optical model as for the other films. The result of the analysis confirmed a low refractive index value ($n_{550} = 2.15$), in accordance with the previously published results [30]. It should be emphasized that all deposited films were optically transparent with extinction coefficient values lower than our instrument detection limit ($k < 10^{-4}$ at 550 nm), as confirmed by absorbance measurements. In addition, none of the investigated films exhibit open porosity, as verified by dynamic ellipsometry measurements performed with an environmental chamber under different dry and humid conditions (not shown here).

In Fig. 1e, we present the measured film hardness (H) values which vary from 7.45 GPa to 7.76 GPa and which present low standard deviations between 0.4 and 1.2%. In a similar trend as that observed for the refractive index (Fig. 1d), H increases with U_C and the lowest value is obtained for the DCMS deposited films at 0.25 Pa while the highest value for the HiPIMS deposited film using 50 Hz at 0.25 Pa. The similarity between refractive index and hardness trends suggests, as stated previously, that the film density increases with U_C and that it is highest in the case of the HiPIMS film using 50 Hz at 0.25 Pa. In fact, the increase of film hardness with packing density has been previously observed by several authors, most notably by Wang et al. [32] for aluminum oxide films fabricated by PECVD. They attributed a decrease in density to gas entrapment or microvoid creation both of which can contribute to a decrease in measured hardness such as that observed in this work.

Fig. 1f shows the dependence of the in-plane mechanical residual stresses obtained from profilometry measurements versus U_C. All the measured stresses were found to be compressive and the HiPIMS- deposited films display significantly lower residual stress than those prepared by DCMS and PDCMS. When comparing the DCMS and the HiPIMS 50 Hz modes, the stress reduction is as high as 60 % at both pressures of 0.80 Pa and 0.25 Pa. This might look

unexpected at first sight. Indeed, most of the ions arriving at the substrates during HiPIMS pulses possess energies ranging from 0 to 100 eV with a maximum below 10 eV [27, 33]. The impact of ions within this energy range as a rule generates compressive stresses due to the surface atoms being subplanted within the growing film [34]. Nonetheless, it has been observed that a small portion ($\leq 1\%$) of highly energetic particles (hundreds to thousands eV) may induce localized long-living thermal spikes in the film, leading to stress relief through atomic rearrangement towards the configuration of lowest bonding and strain energies [34, 35]. This effect was in particular illustrated for amorphous carbon films [35] and amorphous Nb_2O_5 films [30, 36]. Such high-energy particles might be recoiled Ar neutrals originating from ions accelerated towards the target which get neutralized upon impact [24, 37]. They could also be negative O^- ions generated at the cathode surface and accelerated outwards by the potential drop within the cathode sheath. In particular, the presence of high-energy O^- ions was recently demonstrated in reactive HiPIMS process [11, 12], with a pronounced effect on the film structure formation in the case of TiO_2 deposition [11]. Thus, it can be speculated that the observed stress relief is due to O^- ions with a possible contribution of the reflected neutrals.

4. Conclusions

The results of this study demonstrate that despite the differences in the PVD deposition techniques, namely DCMS, PDCMS and HiPIMS, the properties of Ta_2O_5 films prepared at the same average power follow the same tendency of becoming denser, smoother and less stressed with the increase of the discharge voltage. The reason for this appears to be the increasingly significant energetic conditions of the film growth.

In particular, we showed that the HiPIMS-deposited films possess substantially lower surface roughness (~ 0.2 nm) and residual stress (~ -50 MPa), an indication of the synergistic effect of energetic bombardment by both low-energy and high-energy particles. Moreover, we observed that the films prepared by high plasma density HiPIMS discharges operated at a low repetition frequency

($f = 50\,\mathrm{Hz}$), a low working pressure ($p = 0.25\,\mathrm{Pa}$), and a high O_2/Ar gas ratio exhibit refractive index and hardness values ($n_{550} \sim 2.22$, $H \sim 7.8\,\mathrm{GPa}$) comparable to those obtained from thermally-grown oxides. The latter results reveal a very dense, yet relaxed microstructure, which should ensure excellent optical and mechanical stability for these coatings.

Finally, it is worth mentioning that the trends presented here for Ta_2O_5 films prepared by either HiPIMS or other discharge regimes are comparable to those of Nb_2O_5 films investigated in our previous work [14]. This finding suggests that the positive effects of the HiPIMS process on the resulting film properties may also be expected for other amorphous metal oxide materials as well, making them highly suitable for optical coating applications.

Acknowledgments

The authors wish to thank Mr. Soroush Hafezian for his assistance with sample preparation, as well as Mr. Francis Turcot and Mr. Sébastien Chenard for their expert technical assistance. The financial support by NSERC of Canada and by JDSU within the CRDPJ 380174-08 project is gratefully acknowledged. The authors from Polytechnique Montreal are also members of the Quebec Research Cluster on Advanced Materials (RQMP) that benefits from the support by FRQNT of Quebec.

References

[1] J. T. Gudmundsson, N. Brenning, D. Lundin, U. Helmersson, High power impulse magnetron sputtering discharge, J. Vac. Sci. Technol. A 30 (3) (2012) 030801. doi:10.1116/1.3691832.
URL `http://link.aip.org/link/?JVA/30/030801/1`

[2] A. P. Ehiasarian, Plasma surface engineering research and its practical applications, in: R. Wei (Ed.), Reactive Sputter Deposition, Research Signpost, Kerala, India, 2008, pp. 35–85.

[3] A. P. Ehiasarian, J. Wen, I. Petrov, Interface microstructure engineering by high power impulse magnetron sputtering for the enhancement of adhesion, J. Appl. Phys. 101 (5) (2007) 54301.
URL http://dx.doi.org/10.1063/1.2697052

[4] D. A. Glocker, M. M. Romach, D. J. Christie, W. D. Sproul, High power pulsed reactive sputtering of zirconium oxide and tantalum oxide, Society of Vacuum Coaters 47th Annual Technical Conference Proceedings (Dallas, TX).

[5] K. Sarakinos, J. Alami, M. Wuttig, Process characteristics and film properties upon growth of TiO_x films by high power pulsed magnetron sputtering, J. Phys. D: Appl. Phys. 40 (7) (2007) 2108 – 2114.
URL http://dx.doi.org/10.1088/0022-3727/40/7/037

[6] S. Konstantinidis, J. Dauchot, M. Hecq, Titanium oxide thin films deposited by high-power impulse magnetron sputtering, Thin Solid Films 515 (3) (2006) 1182 – 1186.
URL http://dx.doi.org/10.1016/j.tsf.2006.07.089

[7] S. Konstantinidis, A. Hemberg, J. Dauchot, M. Hecq, Deposition of zinc oxide layers by high-power impulse magnetron sputtering, J. Vac. Sci. Technol. B 25 (3) (2007) 19 – 21.
URL http://dx.doi.org/10.1116/1.2735968

[8] V. Sittinger, F. Ruske, W. Werner, C. Jacobs, B. Szyszka, D. Christie, High power pulsed magnetron sputtering of transparent conducting oxides, Thin Solid Films 516 (17) (2008) 5847 – 5859.
URL http://dx.doi.org/10.1016/j.tsf.2007.10.031

[9] F. Ruske, A. Pflug, V. Sittinger, W. Werner, B. Szyszka, D. Christie, Reactive deposition of aluminium-doped zinc oxide thin films using high power pulsed magnetron sputtering, Thin Solid Films 516 (14) (2008) 4472 – 4477.
URL http://dx.doi.org/10.1016/j.tsf.2007.06.019

[10] E. Wallin, U. Helmersson, Hysteresis-free reactive high power impulse magnetron sputtering, Thin Solid Films 516 (18) (2008) 6398 – 6401.

[11] A. Amin, D. Köhl, M. Wuttig, The role of energetic ion bombardment during growth of TiO_2 thin films by reactive sputtering, J. Phys. D: Appl. Phys. 43 (2010) 405303.
URL http://dx.doi.org/10.1088/0022-3727/43/40/405303

[12] K. Sarakinos, D. Music, S. Mráz, M. to Baben, K. Jiang, F. Nahif, A. Braun, C. Zilkens, S. Konstantinidis, F. Renaux, D. Cossement, F. Munnik, J. M. Schneider, On the phase formation of sputtered hafnium oxide and oxynitride films, J. Appl. Phys. 108 (1) (2010) 014904. doi:10.1063/1.3437646.
URL http://link.aip.org/link/?JAP/108/014904/1

[13] M. Aiempanakit, T. Kubart, P. Larsson, K. Sarakinos, J. Jensen, U. Helmersson, Hysteresis and process stability in reactive high power impulse magnetron sputtering of metal oxides, Thin Solid Films 519 (22) (2011) 7779 – 7784.
URL http://dx.doi.org/10.1016/j.tsf.2011.06.021

[14] M. Hála, J. Čapek, O. Zabeida, J. E. Klemberg-Sapieha, L. Martinu, Hysteresis-free deposition of niobium oxide films by hipims using different pulse management strategies, J. Phys. D: Appl. Phys. 45 (5) (2012) 055204.
URL http://stacks.iop.org/0022-3727/45/i=5/a=055204

[15] G. E. Jellison, Jr., F. A. Modine, Parameterization of the optical functions of amorphous materials in the interband region, Appl. Phys. Lett. 69 (1996) 371–373.

[16] W. Oliver, G. Pharr, Improved technique for determining hardness and elastic modulus using load and displacement sensing indentation experiments, J. Mater. Res. 7 (6) (1992) 1564 – 1580.

[17] D. Hensler, J. Cuthbert, R. Martin, P. Tien, Optical propagation in sheet and pattern generated films of ta_2o_5, Appl. Opt. 10 (5) (1971) 1037 – 1042.

[18] G. Oehrlein, F. d'Heurle, A. Reisman, Some properties of crystallized tantalum pentoxide thin films on silicon, J. Appl. Phys. 55 (10) (1984) 3715 – 3725.
URL http://dx.doi.org/10.1063/1.332924

[19] J. Vlček, K. Burcalová, A phenomenological equilibrium model applicable to high-power pulsed magnetron sputtering, Plasma Sources Sci. Technol. 19 (6) (2010) 065010.
URL http://stacks.iop.org/0963-0252/19/i=6/a=065010

[20] J. Emmerlich, S. Mráz, R. Snyders, K. Jiang, J. Schneider, The physical reason for the apparently low deposition rate during high-power pulsed magnetron sputtering, Vacuum 82 (8) (2008) 867 – 870.
URL http://dx.doi.org/10.1016/j.vacuum.2007.10.011

[21] D. Lundin, P. Larsson, E. Wallin, M. Lattemann, N. Brenning, U. Helmersson, Cross-field ion transport during high power impulse magnetron sputtering, Plasma Sources Sci. Technol. 17 (3) (2008) 035021.
URL http://dx.doi.org/10.1088/0963-0252/17/3/035021

[22] J. Čapek, M. Hála, O. Zabeida, J. E. Klemberg-Sapieha, L. Martinu, Deposition rate enhancement in hipims without compromising the ionized fraction of the deposition flux, J. Phys. D: Appl. Phys. 46 (20) (2013) 205205.
URL http://stacks.iop.org/0022-3727/46/i=20/a=205205

[23] D. Horwat, A. Anders, Compression and strong rarefaction in high power impulse magnetron sputtering discharges, J. Appl. Phys. 108 (12) (2010) 123306. doi:10.1063/1.3525986.
URL http://link.aip.org/link/?JAP/108/123306/1

[24] J. A. Thornton, J. L. Lamb, Substrate heating rates for planar and cylindrical-post magnetron sputtering sources, Thin Solid Films 119 (1)

(1984) 87 – 95.
URL http://dx.doi.org/10.1016/0040-6090(84)90160-3

[25] S. M. Rossnagel, J. Hopwood, Magnetron sputter deposition with high levels of metal ionization, Appl. Phys. Lett. 63 (24) (1993) 3285–3287. doi:10.1063/1.110176.
URL http://link.aip.org/link/?APL/63/3285/1

[26] A. P. Ehiasarian, A. Vetushka, A. Hecimovic, S. Konstantinidis, Ion composition produced by high power impulse magnetron sputtering discharges near the substrate, J. Appl. Phys. 104 (8) (2008) 083305.
URL http://dx.doi.org/10.1063/1.3000446

[27] J. Lazar, J. Vlček, J. Rezek, Ion flux characteristics and efficiency of the deposition processes in high power impulse magnetron sputtering of zirconium, J. Appl. Phys. 108 (6) (2010) 063307. doi:10.1063/1.3481428.
URL http://link.aip.org/link/?JAP/108/063307/1

[28] R. Parmentier, F. Lemarchand, M. Cathelinaud, M. Lequime, C. Amra, S. Labat, S. Bozzo, F. Bocquet, A. Charai, O. Thomas, C. Dominici, Piezoelectric tantalum pentoxide studied for optical tunable applications, Applied Optics 41 (16) (2002) 3270 – 3276.

[29] L. Martinu, D. Poitras, Plasma deposition of optical films and coatings: A review, J. Vac. Sci. Technol. A 18 (6) (2000) 2619 – 2645.
URL http://dx.doi.org/10.1116/1.1314395

[30] E. Çetinörgü, B. Baloukas, O. Zabeida, J. E. Klemberg-Sapieha, L. Martinu, Mechanical and thermoelastic characteristics of optical thin films deposited by dual ion beam sputtering, Appl. Opt. 48 (23) (2009) 4536–4544. doi:10.1364/AO.48.004536.
URL http://ao.osa.org/abstract.cfm?URI=ao-48-23-4536

[31] J.-Y. Zhang, I. W. Boyd, Thin tantalum and tantalum oxide films grown by pulsed laser deposition, Appl. Surf. Sci. 168 (14) (2000) 234 – 238.

doi:http://dx.doi.org/10.1016/S0169-4332(00)00605-X.
URL http://www.sciencedirect.com/science/article/pii/S016943320000605X

[32] H. L. Wang, C. H. Lin, M. H. Hon, The dependence of hardness on the density of amorphous alumina thin films by PECVD, Thin Solid Films 310 (1997) 260–264.

[33] A. Hecimovic, A. P. Ehiasarian, Time evolution of ion energies in HIPIMS of chromium plasma discharge, J. Phys. D: Appl. Phys. 42 (13) (2009) 135209.
URL http://dx.doi.org/10.1088/0022-3727/42/13/135209

[34] M. M. M. Bilek, D. R. McKenzie, A comprehensive model of stress generation and relief processes in thin films deposited with energetic ions, Surf. Coat. Technol. 200 (14-15) (2006) 4345 – 4354.
URL http://dx.doi.org/10.1016/j.surfcoat.2005.02.161

[35] M. M. M. Bilek, M. Verdon, L. Ryves, T. W. H. Oates, C. T. Ha, D. R. McKenzie, A model for stress generation and stress relief mechanisms applied to as-deposited filtered cathodic vacuum arc amorphous carbon films, Thin Solid Films 482 (1-2) (2005) 69 – 73.
URL http://dx.doi.org/10.1016/j.tsf.2004.11.159

[36] J. M. Ngaruiya, O. Kappertz, S. H. Mohamed, M. Wuttig, Structure formation upon reactive direct current magnetron sputtering of transition metal oxide films, Appl. Phys. Lett. 85 (5) (2004) 748 – 750.
URL http://dx.doi.org/10.1063/1.1777412

[37] S. M. Rossnagel, Magnetron plasma deposition processes, in: S. M. Rossnagel, J. J. Cuomo, W. D. Westwood (Eds.), Handbook of Plasma Processing Technology: Fundamentals, Etching, Deposition, and Surface Interactions, Noyes Publications, Park Ridge, NJ, 1990, pp. 160–182.